

Article

The Application of Recycled Epoxy Plastic Sheets Waste to Replace Concrete in Urban Construction and Building

Bowen Qi ^{1,2,3}, Shouwu Gao ² and Peilong Xu ^{1,*} ¹ College of Architecture and Urban Planning, Tongji University, Shanghai 200092, China² State Key Laboratory of Bio-Fibers and Eco Textiles, Qingdao University, Qingdao 266071, China³ Shanghai HYP-Arch Design Co., Ltd., Shanghai 200120, China

* Correspondence: xpl@qdu.edu.cn

Abstract: Epoxy plastic, a form of epoxy resin, is widely employed in a variety of sectors due to its superior mechanical qualities and adaptability. The application of waste epoxy plastic in urban highway construction has been a major topic of study. To conduct this study, epoxy polymers are mixed with concrete to enhance the thermal and compressive resistance and tensile strength, which acts as a substitute for conventional cements. The experimental results indicate that ER concrete has good cohesive qualities since it does not collapse or peel, and the nature of the epoxy plastic guarantees that ER concrete has great mechanical capabilities due to the strong bond between the epoxy resin and the fibres. In terms of frost resistance, granular concrete with a 10% ER additive has a mass loss rate between 0.3% and 0.12% and a strength loss rate between 3.55 and 9.4%, outperforming conventional concrete. When often loaded by traffic, ER concrete exhibits no substantial permanent deformation, and its fatigue damage rate is superior to that of ordinary concrete. In total, 10% admixture of ER concrete may efficiently fulfil BPN (British Pendulum Number) and structural depth standards, while greatly improving the road's skid resistance. In addition, its modulus of elasticity, deformation capacity, and high-temperature stability are superior to those of conventional concrete.

Keywords: epoxy resin; new concrete; road construction; reusable



Citation: Qi, B.; Gao, S.; Xu, P. The Application of Recycled Epoxy Plastic Sheets Waste to Replace Concrete in Urban Construction and Building. *Processes* **2023**, *11*, 201. <https://doi.org/10.3390/pr11010201>

Academic Editors: Elsayed Elbeshbishy and Farokh Laqa Kakar

Received: 22 November 2022

Revised: 29 December 2022

Accepted: 31 December 2022

Published: 8 January 2023



Copyright: © 2023 by the authors. Licensee MDPI, Basel, Switzerland. This article is an open access article distributed under the terms and conditions of the Creative Commons Attribution (CC BY) license (<https://creativecommons.org/licenses/by/4.0/>).

1. Introduction

China's development in the 21st century has been marked by fast expansion and extensive building, which use a growing quantity of mineral resources. Traditional building materials are insufficient to keep up with technological advancements; thus, novel building materials are on the rise in the construction and engineering sectors [1–5]. Epoxy plastics are epoxy resin-based plastics, which are essentially polymeric compounds of epoxy resin materials. Epoxy plastics are widely used in various fields, such as coatings and composites, due to their excellent mechanical structure, adhesion, and chemical stability. However, the waste of epoxy plastics and the waste disposal methods, such as incineration and landfill, damage ecological resources, and severely pollute the ecological environment [6,7]. China is the world's largest producer of epoxy resins, and, based on the 14th Five-Year Plan, it is even more important to achieve the recycling of epoxy resins and their by-products. At present, most of the domestic epoxy resin production is still in the middle- and low-end of the industry chain, with insufficient R&D and innovation capabilities, and excess production capacity of middle- and low-end products [8]. In order to reuse epoxy resins, research has been undertaken on the utilisation of waste-recovered epoxy resins in urban building. Epoxy plastic sheets are broken and filled with various materials using mechanical recycling techniques. Epoxy resins are promoted by the reuse of epoxy plastic as a high-performance, multi-directional, pollution-free, and low-cost industry.

2. Related Works

Epoxy resins have advanced significantly as a result of the development of new energy sources and new materials, according to researchers throughout the world. On the basis of the material's material stability, corrosion resistance, tensile strength, and non-flammability, a number of performance enhancement methods have been implemented. The findings of the experiment demonstrated that the tensile strength of the polymer matrix material was significantly enhanced [9]. Fernández-Ruiz et al. utilised epoxy resin and tyre powder as substitutes for cement when mixing concrete. The results demonstrated that the use of polymer cement concrete altered the peak post slope of the stress-strain curve, indicating improved ductility, which is particularly important in seismic engineering [10]. Gao et al. developed a novel technique for measuring the delamination strength of rare earth barium copper oxide (REBCO)-coated conductors (CC) with shear interfaces [11]. As demonstrated by the experimental results, the extreme dispersion of the test data, exhibited by conventional testing techniques, has been eliminated. Juliano et al. evaluated the commercial applications of HTL that depolymerizes synthetic waste polymers into biocrude or platform chemicals by analyzing the commercial applications of mixed plastic waste treated by hydrothermal liquefaction for sustainable biocrude production [12,13]. The experiment demonstrates how HTL depolymerizes a variety of synthetic polymers and identifies the polymers that are most desirable or unsuitable for subcritical processing. Yuan et al. employed epoxy resin as the joint lubricant to optimise and enhance the strength of segmental concrete bridges [14]. In the test result, the shear strength, failure mode, and ductility of epoxy resin joints were altered. Yousef et al. synthetically utilised the pyrolysis products from the pyrolysis of plastic waste by refining and reprocessing the carbon from the plastic waste into carbon pellets, which were then utilised as micro-fillers for lightweight material applications [15]. According to experimental findings, the panels' modulus of elasticity increased by 22% compared to the samples. At the same FBC concentration, thermal stability, and energy impact absorption improved by 21% (in the main decomposition zone) and 38%, respectively. According to research, epoxy resins have a wide variety of uses in many sectors and may be employed in urban building by altering their mixing ratios.

For urban building projects, builders are progressively using new forms of concrete [14]. To compute the interfacial shear and normal stresses in RC-plated beams, Gueñeche et al. provide an efficient study of shear deformation based on a two-dimensional elastic theory technique [16]. Typically, fibre-reinforced polymers (carbon or glass) or steel are used to produce the plate material necessary to strengthen the beams. The experimental results indicate that all plated beams may be utilised, and the numerical values obtained are comparable with actual applications. Wang et al. used fly ash, fibres, magnesium oxide, and shrinkage-reducing additives to enhance the frost resistance of concrete in cold climates [17]. According to the results, the addition of fly ash and fibres to fresh concrete might effectively increase its resistance to severe frost damage. Jenness and Shukla advocated incorporating bio-inspired catechol-like molecular binders into aggregate mixtures of concrete in order to enhance its adherence [18]. The results indicated that dopamine molecules would be the optimal choice for enhancing adhesion in concrete mixtures containing such materials. According to Nelubova, mineral modifiers can be generated by mechanically activating amorphous raw materials in an aqueous environment in order to improve the performance of autoclave-hardened gas concrete [19]. The improved pore dialogue process in gas concrete mixes ensured the creation of pore structures in the composites, and it was feasible to increase the concrete's strength with the addition of active additives while boosting its thermal insulation. Varghese et al. studied the addition of nano-sized silica into concrete to enhance attributes, such as compressive strength and tensile strength at fracture [20]. The silica nano-concrete has superior mechanical qualities, a high compressive strength, and maturity to facilitate building activities on-site, but it also exhibits more creep and dry shrinkage.

Academics have conducted extensive studies on the recyclability of waste epoxy resin and the improvement of traditional concrete, but there is less research on the mix of waste epoxy resin into concrete. Despite the fact that China is a major producer of epoxy resin, the epoxy resin concrete market is relatively small. Through the application research of waste recycled epoxy plastic sheets in lieu of concrete in urban construction buildings, this work presents a theoretical reference for high-performance green urban construction development design.

3. A New Concrete Model with Used Recyclable Epoxy Plastic Sheets

Epoxy resin with a stable structure is widely utilised in the aerospace and paint sectors due to its superior processability, heat resistance, and corrosion resistance. Epoxy resin generates massive amounts of trash. Epoxy resin waste management is a concern for all sectors. Due to the cross-linked network structure of conventional epoxy resin, however, it will be unable to dissolve and reprocess it after curing, making the development of reusable epoxy resin a formidable issue [21,22]. When epoxy resin is recycled, the third level of recycling is mostly utilised to manufacture fuel; however, the fourth level of recycling is more environmentally damaging [23]. Therefore, the second level of recycling (mechanical recycling) is adopted, and the waste of epoxy plastic plates is mixed into the concrete by adding new materials and additives after crushing and rolling, which can enhance the concrete's compressive and tensile strengths. However, when the plastic is crushed under the influence of mechanical force, surface fractures will form. Figure 1 illustrates the primary types of microcracks.

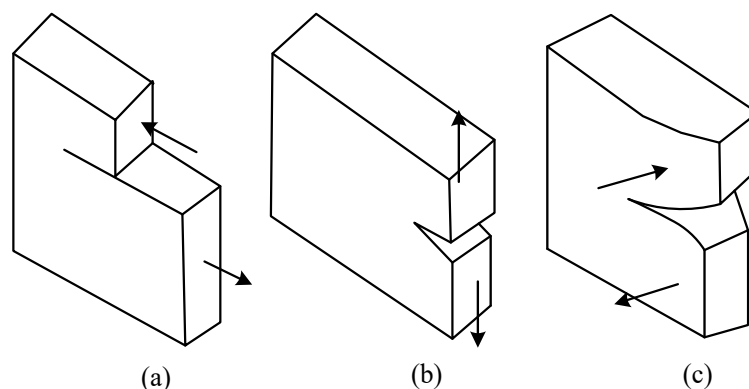


Figure 1. Crack fracture mode. (a) tensile (b) sliding (c) tearing.

In the crushing process, the strain on the plastic is unequal, leading to the following three distinct types of fractures under the influence of mechanical force: tensile (a), sliding (b), and tearing (c). The mixed mode crack of the first two crack combinations in comminution is the focus of this research. The maximum circumferential stress criteria and the strain energy density criterion are utilised to determine the mixed mode fracture's propagation.

$$\sigma_{\theta} = \frac{1}{2\sqrt{2\pi r}} \cos \frac{\theta}{2} \left[K_1 \cos^2 \frac{\theta}{2} - \frac{3}{2} K_2 \sin \theta \right] \quad (1)$$

$$\tau_{r\theta} = \frac{\cos \frac{\theta}{2}}{2\sqrt{2\pi r}} [K_1 \sin \theta + K_2(3 \cos \theta - 1)] \quad (2)$$

In Equations (1) and (2), the tip stress field in polar coordinates, K_1 , K_2 represent the two types of cracks. The maximum stress direction can be determined from Equation (3).

$$\frac{\partial \sigma_{\theta}}{\partial \theta} = 0, \quad \frac{\partial^2 \sigma_{\theta}}{\partial \theta^2} < 0 \quad (3)$$

The critical conditions for fracture are obtained by associating Equation (1) with Equation (3) to obtain the direction of the cracking angle based on the critical stress intensity factor as in Equation (4).

$$\cos \frac{\theta_0}{2} \left[K_1 \cos^2 \frac{\theta_0}{2} - \frac{3}{2} K_2 \sin \theta_0 \right] = K_{Ic} \quad (4)$$

In Equation (4), θ_0 represents the direction of the cracking angle and K_{Ic} is the critical stress intensity factor. The tangential velocity of the epoxy plastic is shown in Equation (5) due to the high hardness of the epoxy plastic and the need to obtain the required particle size through the following two methods: coarse and fine crushing.

$$v_r = n\pi d/60 \quad (5)$$

In Equation (5), n is the speed of rotation of the knife teeth for the control of mechanical forces in the shredder and d is the diameter of rotation.

Cement is the most significant component of concrete. After combining with aggregate and undergoing a hydration process, it can harden into a matrix with a high strength. The epoxy plastic plates may also be reused by incorporating them into concrete to assure the strength of epoxy resin concrete (ER concrete), but they must pass the concrete compressive strength test [24]. The study selected a fibre epoxy composite board with a density of 1.982 g/m^3 provided by the insulation material company. The ER concrete used in the experiment is a prism with 100 mm long sides on both the big and small sides. The ER concrete mixture is depicted in Table 1.

Table 1. Proportion of ER concrete mix with various epoxy plastic board dose and particle size.

Number	Water (kg/m ³)	Cement (kg/m ³)	Sand (kg/m ³)	Gravel (kg/m ³)	ER		
					Size	Proportion (%)	Mixing Amount (kg/m ³)
Z	185	420	580	1230	/	/	/
A1	185	420	552	1230	Category A	5	17.25
A2	185	420	523	1230		10	34.47
A3	185	420	495	1230		15	52.5
B1	185	420	552	1230	Category B	5	15
B2	185	420	523	1230		10	30
B3	185	420	495	1230		15	45
C1	185	420	552	1230	Category C	5	16
C2	185	420	523	1230		10	32
C3	185	420	495	1230		15	48

Three types of ER are added, as shown in Table 1, Z is the proportion of conventional concrete used as the experiment's control group, and A1–C3 is the number of unique test pieces. The compressive strength formula for the compression test of ER concrete is shown in Formula (6).

$$f_{ce} = f_{cc} \times 0.95 \quad (6)$$

In Equation (6), f_{ce} is the cubic compressive strength of ER concrete and f_{cc} is the value measured in the experiment. The conversion factor is set at 0.95. When calculating the splitting and tensile strength of ER concrete, the formula is shown in Equation (7).

$$f_{ts} = f_m \times 0.85 \quad (7)$$

In Equation (7), f_{ts} is the resistance strength (MPa) and f_m is the value measured in the experiment with a conversion factor of 0.85.

After selecting the proper ratio of cement, crushed treated epoxy plastic, water, and other fundamental elements, proportionate mixing, and referencing the abrupt ordinary concrete design technique for ER concrete design strength, derive the strength formula as given in Formula (8).

$$f_{(cu,o)} = f_{(cu,k)} + 1.645\sigma \quad (8)$$

In Equation (8), $f_{(cu,o)}$ is the pre-set strength of ER concrete, $f_{(cu,k)}$ is the standard value of the compressive strength of ER concrete prisms, and σ is the standard deviation of strength. The standard deviation of strength is defined by Equation (9).

$$\sigma = \sqrt{\frac{\sum_{i=1}^n f_{cu,i}^2 - nm_{f_{cu}}^2}{n-1}} \quad (9)$$

In Equation (9), $f_{cu,i}$ is the strength test (MPa) of the ER concrete for the i experiment, n is the number of ER concrete strength experiments, and $m_{f_{cu}}$ is the average of the strengths of the test samples from the m group. The durability of the concrete is dependent on the ER concrete water–cement ratio. The smaller the water–cement ratio, the stronger the bond and the greater the strength develops, and vice versa. The formula for calculating the water-to-ash ratio is shown in Equation (10).

$$W/C = \frac{\alpha_a f_{ce}}{f_{cu,o} + \alpha_a \alpha_b f_{ce}} \quad (10)$$

In Equation (10), W/C is the water-to-ash ratio and the regression coefficients are α_a , α_b . f_{ce} is the value of ER concrete when it is tested for 28-day compressive strength and is calculated by Equation (11).

$$f_{ce} = \gamma_c f_{ce,g} \quad (11)$$

In Equation (11), γ is the enrichment factor and $f_{ce,g}$ is the value of the strength class. ER concrete is used in urban construction cases where the compressive strength is greater, such as roads and floors. The final sand rate of ER concrete is determined after the concrete water consumption is set at a lower slump, as shown in Equation (12).

$$S_p = \partial \frac{P\rho'_s}{P\rho'_s + \rho'_g} \quad (12)$$

In Equation (12), S_p is the final sand rate, P is the porosity of the coarse aggregate, the stockpile density of sand and gravel is ρ'_s , the stockpile density of stone is ρ'_g , and the enrichment factor of cement paste is ∂ . The porosity equation is shown in Equation (13).

$$P = \left(1 - \frac{\rho'_g}{\rho_g}\right) \quad (13)$$

In Equation (13), ρ_g is the apparent density of the stone.

When calculating the granular loose material that acts as a skeleton or filler in ER concrete, the aggregate is determined by the volumetric method and the formula is shown in Equation (14).

$$\begin{cases} \frac{M_s}{M_s + M_g} = S_p \\ \frac{W}{\rho_w} + \frac{C}{\rho_c} + \frac{M_s}{\rho_s} + \frac{M_g}{\rho_g} + 0.01\alpha = 1 \end{cases} \quad (14)$$

In Equation (14), M_s is the amount of sand in the concrete, ρ_w is the apparent density of sand, M_g is the amount of stone, ρ_c is the apparent density of stone, W is the amount

of water, and C indicates the amount of cement. The apparent density of ER concrete is calculated according to Equation (15).

$$\rho = \frac{m_2 - m_1}{V} \quad (15)$$

In Equation (15), ρ is the apparent density of ER concrete, m_1 is the mass of the mixing drum, and m_2 is the total mass of concrete and mixing drum.

The waste epoxy plastic sheets are crushed and mixed into concrete instead of traditional concrete used for road and floor construction. It is essential to test new ER concrete. Compressive strength is the most basic mechanical property index test for concrete, and the formula for compressive ultimate strength of concrete is shown in Equation (16).

$$f_{ce} = \frac{F}{A} \quad (16)$$

In Equation (16), f_{ce} is the strength test value, F is the breaking load, and A is the compressive area of ER concrete. To test the splitting tensile strength, the formula is shown in Equation (17).

$$f'_{ts} = \frac{2F}{\pi A} \quad (17)$$

In Equation (17), f'_{ts} is the tensile strength, which can be combined with Equation (7) to find the strength of ER concrete. In the high temperature performance test, epoxy resin is used as a thermoplastic material. In order to keep the deformation resistance of ER concrete under high temperature conditions, the rutting test is conducted with the indoor test method. The test environment is 60 °C, the wheel pressure is 0.7 MPa, and the speed of rolling the test block is 42 times per minute. Following the test, the rut depth of the 45 min rolling test block and the 60 min rolling test block is sorted out. Consequently, the formula for calculating dynamic stability is presented in Formula (18).

$$DS = \frac{(t_1 - t_2) \times N}{d_1 - d_2} c_1 \times c_2 \quad (18)$$

In Formula (18), DS is the dynamic stability and $t_1 - t_2$ is the time to take the rut depth. c is the experimental parameter, which is taken as 1, N is the speed of rolling test block, and $d_1 - d_2$ is the rutting depth at different times.

4. Property Research Analysis of Concrete Mixed with Recycled Epoxy Plastic Sheets

In this study, the tensile and compressive resistance, damage resistance, and high temperature resistance of the new ER concrete with recycled epoxy plastic plate crushed into concrete were analyzed, and data were used to support the analysis [25]. Workability refers to the ability of fresh cement concrete to be easy to operate in each process and to obtain uniform quality and dense formation, also known as the workability of concrete. The workability of a concrete mixture is a comprehensive concept, so the slump test is used to determine the shaping and pumping ability of a concrete mixture. Slump is an important indicator to measure whether a certain concrete can meet the standard operation and judge whether the construction can progress normally. In different construction operations, the requirements for slump are also different. Generally, slump is measured by a quantitative index, which directly reflects the shaping capacity and pumping capacity of concrete. The ER concrete studied in this study is used in nonbearing structures, such as similar highways, and the slump is selected to be low. The comparison curve of slump with different dosages and particle sizes is shown in Figure 2.

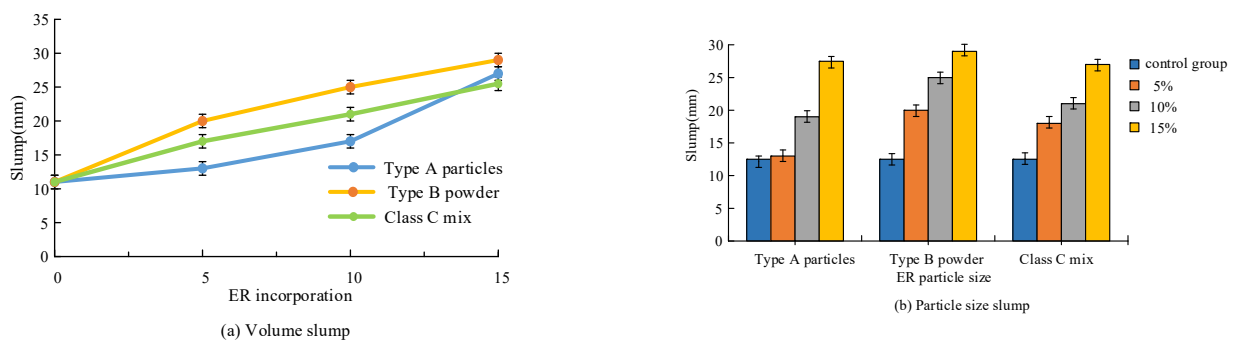


Figure 2. Comparison curve of slump with different dosage and particle size.

As the epoxy plastic sheet is composed of epoxy resin by nature, its type may be determined based on Figure 2's comparison, as it is an epoxy plastic (a). An A particle increases somewhat with 5% admixture, followed by steeper curves, and a larger slump to 27. The slump degree of class B powder, despite being the largest, increases to 29 at the slowest rate. The C powder-particle demonstrates a range of slump classes. In Figure 2b of the particle size slump comparison, the control group consists of typical concrete with a slump of 12.5 when A particles are mixed at 5%, and an increase of 14 is observed when blended at 15%. When class B powder was mixed at a ratio of 5%, the slump was 20.7 percentage points more than normal concrete. The degree of decline also rose by seven when combined. Compared to normal concrete, the slump rose by 5% at 5% and 13% at 15%.

The compressive strength of conventional concrete and ER concrete with various additives is compared in Table 2. At 7 D, 14 D, and 28 D, the compressive strengths of conventional concrete were 30, 7, 34.01, and 38.01, respectively. In total, a 5% admixture enhanced the compressive strength of class A granules relative to conventional concrete by 5.9–17.89%. The greatest notable rise in compressive strength was recorded at 10% when it rose from 13.97% to 26.41 percent. The compressive strength rose from 2.18 percent to 12.65 percent when 15% class A particles were introduced. Class B powder's compressive strength rose by 1.6619.05% when combined at 5%, 7.1322.15% when mixed at 10%, and 1.9921.26% when mixed at 15%, compared to normal concrete. The compressive strength improved from 7.62 percent to 19.14 percent at 5%, from 10.55 percent to 15.97 percent at 10%, and from 0.36 percent to 16.5 percent at 15% of the mixture. It can be shown that as the amount of admixture increases, so does the compressive strength of ER concrete. When waste plastic is crushed into a granular form and a 10% admixture is added, the total compressive strength is greater than the compressive strength of powdered waste plastic. Due to the nature of the epoxy plastic, the high degree of adhesion between the epoxy resin and the fibres promotes superior mechanical qualities in ER concrete, which exhibits a greater compressive strength than traditional concrete.

Table 2 displays the compressive strength extreme difference analysis performed by the MinitabR20 software for the admixture level and particle size of the crushed particles in order to calculate the quantities of epoxy plastic used in ER concrete. As shown in Table 3, during the 7-day tensile test, the three doping levels were 32.5, 33.4, and 31.7, with a polar difference of 1.73, but the particle size levels were 32.9, 31.9, and 32.6, with a polar difference of 0.9. The polar difference for the 14-day tensile test was 1.77 for the three degrees of doping and 2.30 for the three particle sizes. As the particle size has a greater impact on the compressive strength than the admixture, class A granular concrete is more likely to increase the tensile strength of conventional concrete.

Table 2. Compressive strength range analysis table.

Number	/	Compressive Strength			
		Proportion (%)	7 D	14 D	28 D
Ordinary concrete	/		30.7	34.01	38.01
Type A particles	5%		32.51	39.72	44.81
	10%		34.99	40.44	48.05
	15%		31.37	37.59	42.82
Type B powder	5%		31.21	38.82	45.25
	10%		32.89	40.86	46.43
	15%		31.31	45.83	46.09
Class C mix	5%		33.04	40.52	43.29
	10%		33.94	42.92	44.08
	15%		30.81	38.08	44.31

Table 3. Comparison of mass loss rate and strength loss rate of ER concrete with different contents.

/		7 DAYS	14 DAYS
		Dosage	Average K1
	Average K2	33.4	41.3
	Average K3	31.7	40.2
	Range R	1.73	1.77
Particle size	Average K1	32.9	39.2
	Average K2	31.9	41.4
	Average K3	32.6	40.2
	Range R	0.90	2.3

Figure 3 illustrates the comparative splitting tensile strengths of 7 d and 14 d ER concrete. The standard concrete has a strength of 3.45 MPa at 7 d and 4.08 MPa at 14 d. In the experiment comparing 7 d concretes, the splitting tensile strength of the class A granules rose with an increasing admixture level, reaching a maximum value at 10% admixture level and then falling marginally when it exceeded 10%. In the experiment comparing concretes at 14 d, the splitting tensile strength of the class A particles rose, with the same general trend as at 7 d. At 10%, the splitting tensile strength reaches its maximum and then declines slightly. The splitting tensile strength was greatest at 10% and declined somewhat as the quantity of additive increased. The class C mix strength recorded its greatest value of 5% and its lowest value of 10%. As the quantity of admixture is increased, the splitting tensile strength progressively recovered and increased, but remained below that of the control concrete. This is the general state of the splitting tensile strength of the two types of concrete produced by mixing the class B and class C powders. The compressive strength was less than that of granular concrete of class A. When the ER admixture was chosen as granular and the admixture quantity was 10%, the greatest experimental data and best outcomes were produced.

The mass loss rate and strength loss rate of ER concrete with various admixture types and quantities are displayed in Table 4. As indicated in the table, according to the specification, the frost strength loss rate for pavement concrete should be less than 20%, and the mass loss should be less than 5%. Class A granular concrete has a mass loss rate between 0.3% and 0.12%, and a strength loss rate between 3.55 and [*]. The maximum mass loss rate of the class B powdered concrete is 0.53% at 15% admixture, whereas the

maximum strength loss rate is 9.09% at 5% admixture. The mass loss rate of the class C mixed concrete spans from 0.02% to 0.74%, while the strength loss rate has a minimum range between 1.27% and 1.51%. All three varieties of ER concrete are more frost-resistant than conventional concrete and are guaranteed to remain safe and undamaged for the rest of their operational life.

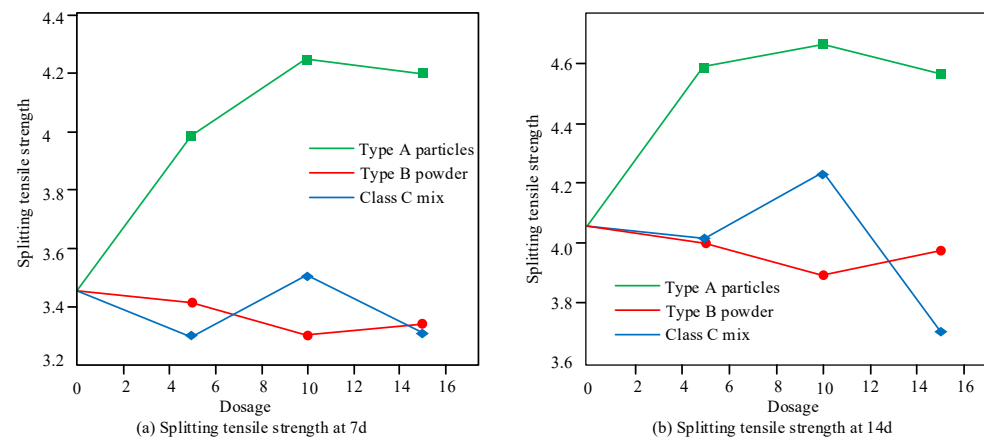


Figure 3. Splitting tensile strength of ER concrete.

Table 4. Mass loss rate and strength loss rate of ER concrete.

Category	Incorporation Amount	Mass Loss Rate (%)	Strength Loss Rate (%)
Type A particles	5%	0.3	9.4
	10%	0.18	3.55
	15%	0.12	4.86
Type B powder	5%	0.34	9.09
	10%	0.14	8.85
	15%	0.53	7.59
Class C mix	5%	0.74	1.51
	10%	0.53	1.27
	15%	0.02	1.35

The doping level and particle size of the crushed particles are displayed in Table 5 to determine the doping level and particle size of the epoxy plastic used in ER concrete. This is shown in Table 5 for the 7-day tensile test. All three levels of doping were around 3.5, with an extreme difference of 0.12, but the particle size levels were 4.147, 3.351, and 3.369, with an extreme difference of 0.80. The extreme difference for the 14-day tensile test was 0.18 for the three doping levels and 0.65 for the three particle sizes. Due to the effect of particle size on tensile strength, the class A granular concrete is more likely to increase the tensile strength of ordinary concrete. The best results for ER concrete were obtained by selecting the class A granular concrete with a 10% admixture rate based on the findings of the extreme difference study and the mean values in Tables 3 and 5.

Figure 4 depicts the fatigue damage rate of three types of ER concrete and a rice husk concrete with varying mixing amounts during the following year. Among the three types of ER concrete with a 5% mixing ratio, the fatigue damage rate of the class A granular concrete is the lowest. The fatigue damage rate of the class B powdered concrete reaches 190–195 when the mixing quantity exceeds 10 percent. When the mixing ratio reaches 15%, the damage rate of all three types of ER concrete lowers and falls below 190. When the driving force is frequently applied, the fatigue cracking degree of the three ER concretes is smaller, and there will be no substantial permanent deformation. In comparison to prior

trials, the fatigue damage rate of the three ER concretes is less than 170 when 10% A-type particles are introduced.

Table 5. Average and range of two variables' influence on tensile strength.

		7 DAYS	14 DAYS
Dosage	Average K1	3.562	4.206
	Average K2	3.687	4.269
	Average K3	3.616	4.086
	Range R	0.12	0.18
Particle size	Average K1	4.147	4.612
	Average K2	3.351	3.959
	Average K3	3.369	3.991
	Range R	0.80	0.65

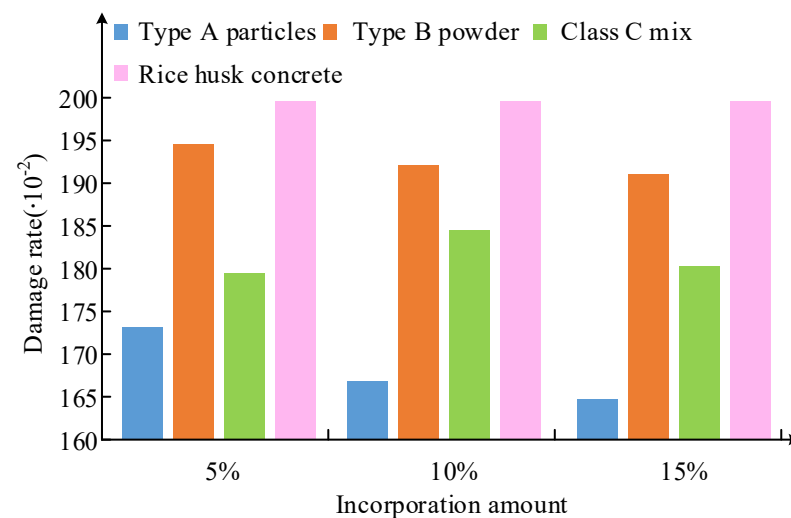


Figure 4. Comparison diagram of fatigue damage rate of concrete and rice husk concrete in this study.

Figure 5 demonstrates the BPN values and construction depth of regular concrete with class A particles at 5–15% admixture and class C mixed concrete at 5% admixture in ER concrete. It can be observed that when epoxy plastic is combined with concrete, the BPN values and construction depth decrease significantly, but still fulfil the specifications. The BPN and construction depth criteria may be adequately met when class A concrete is mixed at a proportion of 10%. At a powder mixture of between 15% and 5%, both the construction depth and the BPN drop. At 15%, the epoxy plastic completely saturates and fills the spaces in regular concrete. Consequently, some bonding materials overflow and filled the surface air, resulting in a minor decrease in slip resistance. Following this, an increase in admixture will further diminish slip resistance and building depth. Therefore, a 10% class A granular concrete additive is the optimal choice for ER concrete.

Figure 6 compares the dynamic stability of 5–15% class A granular concrete and 5% class C powder concrete with that of conventional concrete. The range of dynamic stability of the concrete is less than 3000. Thus, the cured epoxy plastic granules have a high modulus of elasticity and a greater capacity for deformation. It also meets the requirements for road paving and road rehabilitation in terms of high-temperature stability. Additionally, epoxy plastic granules can be used as an alternative to conventional concrete.

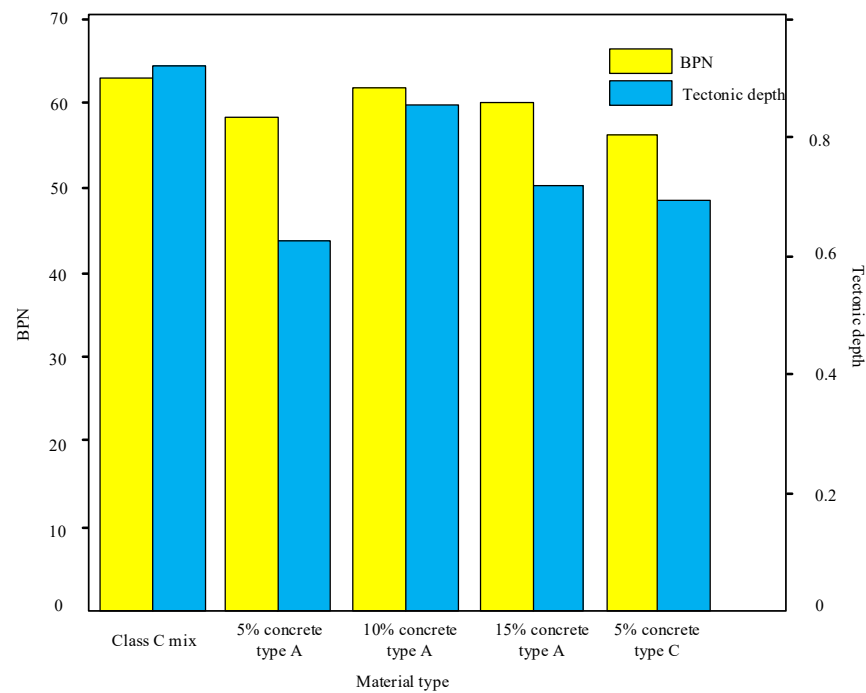


Figure 5. Slip resistance of ER concrete.

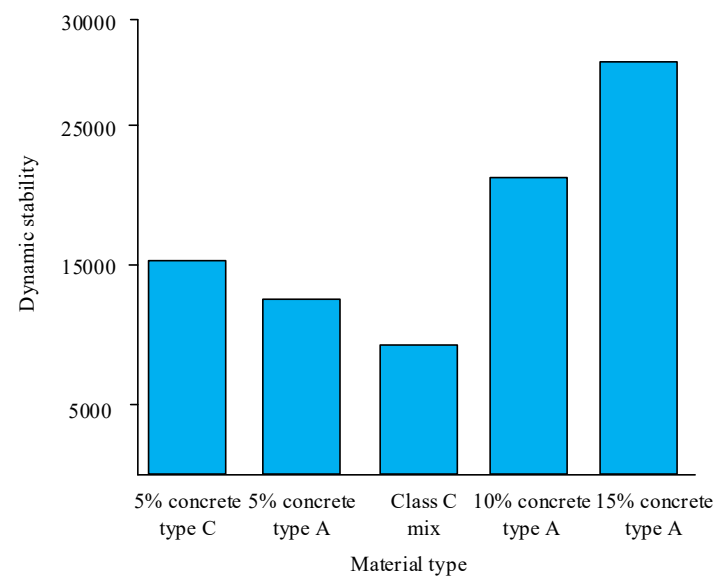


Figure 6. Dynamic stability of concrete with different ER.

5. Conclusions

Epoxy plastic sheet recycling is an ongoing issue for a green and sustainable society. At the same time, conventional building materials are increasingly unable to keep up with the latest developments in industrial technology. This study mixes epoxy plastic sheets into the concrete in order to increase the tensile and compressive strength, fragility, heat resistance, and other features to design a new ER concrete for urban engineering and the construction of roads and floors. The experimental research revealed that ER concrete did not slump or break, showing strong cohesive characteristics. Due to the nature of the epoxy plastic epoxy resin and the high bond between the fibres to ensure a high mechanical performance in ER concrete, the compressive capacity has a superior performance compared to conventional concrete when the waste plastic is crushed into a granular form and the admixture amount reaches 10%. Adding 10% admixture enhances the splitting tensile strength of ER granular

concrete, whereas the splitting compressive strength of powder type and powder granular mix concrete is lower than that of granular concrete. When granular ER admixture was selected at a concentration of 10%, the best outcomes were obtained. In the frost resistance studies, the mass loss rate of granular concrete varied from 0.3% to 0.12%, and the strength loss rate ranged from 3.55 to 9.4%; both were stronger than conventional concrete in terms of frost resistance, assuring the safety and integrity of the concrete throughout its service life. Under repeated traffic loads, ER concrete does not exhibit substantial permanent deformation, and its fatigue damage rate performs even better. When granular concrete is mixed at 10%, the BPN and construction depth criteria may be met efficiently, and the road's skid resistance is greatly enhanced. It has a larger modulus of elasticity and more deformability than conventional concrete, as well as excellent stability at high temperatures. However, only three types of ER concrete have a mix fraction of less than 20%, and there are a limited number of types. Consequently, raising the replacement ratio of concrete is also one of the future research goals, and the assessment of durability in concrete is insufficient, which will be future research area.

Author Contributions: Conceptualization, P.X.; methodology, P.X.; formal analysis, B.Q. and S.G.; data curation, S.G.; writing—original draft preparation, B.Q.; writing—review and editing, P.X. All authors have read and agreed to the published version of the manuscript.

Funding: This paper is supported by the Ministry of Education University-Industry Collaborative Education Program (202101326005, 202102295003) and 2019, 2020 Innovative Experimental Teaching Project of Qingdao University.

Institutional Review Board Statement: Not applicable.

Conflicts of Interest: The authors declare no conflict of interest.

References

1. Xu, N.; Yang, Y.; Peng, M. Toward the threshold of radiation hazards of U in Chinese coal through the CART algorithm. *Environ. Sci. Technol.* **2022**, *56*, 1864–1874. [[CrossRef](#)] [[PubMed](#)]
2. Gounni, A.; Mabrouk, M.T.; El Wazna, M.; Kheiri, A.; El Alami, M.; El Bouari, A.; Cherkaoui, O. Thermal and economic evaluation of new insulation materials for building envelope based on textile waste. *Appl. Therm. Eng.* **2019**, *149*, 475–483. [[CrossRef](#)]
3. Wood, S. Building new knowledge of advanced materials in extreme environments. *Mater. Aust.* **2020**, *53*, 38.
4. Xu, P.; Cui, L.; Gao, S.; Na, N.; Ebadi, A.G. A theoretical study on sensing properties of in-doped ZnO nanosheet toward acetylene. *Mol. Phys.* **2022**, *120*, e2002957. [[CrossRef](#)]
5. Huang, Y.; Zhang, W.; Liu, X. Assessment of Diagonal Macrocrack-Induced Debonding Mechanisms in FRP-Strengthened RC Beams. *J. Compos. Constr.* **2022**, *26*, 04022056. [[CrossRef](#)]
6. Stochioiu, C.; Deca, A.; Hadar, A.; Gheorghiu, H. In-plane Shear Response of a Flax Fiber-epoxy Resin Composite Subjected to Repeated Loading and Creep-recovery Cycles. *Mater. Plast.* **2021**, *58*, 179–186. [[CrossRef](#)]
7. Group, J. METI seeks to scale up demonstration testing in plastic recycling project. *Jpn. Chem. Dly.* **2021**, 1–2.
8. Wang, Z.; Chen, Y.; Chen, S.; Chu, F.; Zhang, R.; Wang, Y.; Fan, D. Preparation and characterization of a soy protein based bio-adhesive cross linked by waterborne epoxy resin and polyacrylamide. *RSC Adv.* **2019**, *60*, 35273–35279. [[CrossRef](#)]
9. Lokesh, K.S.; Shrinivasa, M.D. Effect of bio-filler on tensile and compressive behavior of bidirectional e-glass reinforced with epoxy plastics. *J. Plast. Polym. Technol.* **2020**, *1*, 11–19.
10. Fernández-Ruiz, M.; Gil-Martín, L.; Carbonell-Márquez, J.; Hernández-Montes, E. Epoxy resin and ground tyre rubber replacement for cement in concrete: Compressive behaviour and durability properties. *Constr. Build. Mater.* **2018**, *173*, 49–57. [[CrossRef](#)]
11. Gao, P.; Geng, X.; Man, G.; Wang, X. Measurement of shear delamination strength of REBCO coated conductors. *IEEE Trans. Appl. Supercond.* **2022**, *32*, 1–5. [[CrossRef](#)]
12. Dos Passos, J.S.; Glasius, M.; Biller, P. Screening of common synthetic polymers for depolymerization by subcritical hydrothermal liquefaction. *Process Saf. Environ. Prot.* **2020**, *139*, 371–379. [[CrossRef](#)]
13. Chen, Y.; Ma, K.; Xu, P.L.; Si, H.; Duan, Y.B.; Zhai, H. Design and Screening of New Lead Compounds for Autism Based on QSAR Model and Molecular Docking Studies. *Molecules* **2022**, *27*, 7285. [[CrossRef](#)]
14. Yuan, A.; Yang, C.; Wang, J.; Chen, L.; Lu, R. Shear Behavior of Epoxy Resin Joints in Precast Concrete Segmental Bridges. *J. Bridg. Eng.* **2020**, *139*, 371–379. [[CrossRef](#)]
15. Yousef, S.; Eimontas, J.; Subadra, S.P.; Striūgas, N. Functionalization of char derived from pyrolysis of metallised food packaging plastics waste and its application as a filler in fiberglass/epoxy composites. *Process. Saf. Environ. Prot.* **2021**, *147*, 723–733. [[CrossRef](#)]

16. Zhang, W.; Huang, Y. Three-dimensional numerical investigation of mixed-mode debonding of FRP-concrete interface using a cohesive zone model. *Constr. Build. Mater.* **2022**, *350*, 128818. [[CrossRef](#)]
17. Guenaneche, B.; Benyoucef, S.; Tounsi, A.; Adda Bedia, E.A. Improved analytical method for adhesive stresses in plated beam: Effect of shear de-formation. *Adv. Concr. Constr.* **2019**, *7*, 151–166.
18. Wang, L.; Guo, F.X.; Yang, H.M.; Wang, Y.; Tang, S.W. Comparison of FLY ASH, PVA Fiber, MgO and Shrinkage-reducing Admixture on the Frost Resistance of Face Slab Concrete via Pore Structural and Fractal Analysis. *Fractals* **2021**, *29*, 2140002. [[CrossRef](#)]
19. Jenness, G.R.; Shukla, M.K. Effect of concrete composition on the thermodynamic binding of dopamine: A DFT Study. *Langmuir* **2021**, *38*, 472–481. [[CrossRef](#)]
20. Nelubova, V.V. The composition and properties of autoclaved gas concrete with amorphized raw modifiers. *Mater. Sci. Forum.* **2020**, *947*, 142–148. [[CrossRef](#)]
21. Varghese, L.; Rao, V.V.L.K.; Parameswaran, L. Nanosilica-added concrete: Strength and its correlation with time-dependent properties. *Proc. Inst. Civ. Eng. Constr. Mater.* **2019**, *172*, 85–94. [[CrossRef](#)]
22. Venezia, V.; Matta, S.; Lehner, S.; Vitiello, G.; Costantini, A.; Gaan, S.; Malucelli, G.; Branda, F.; Luciani, G.; Bifulco, A. Detailed thermal, fire, and mechanical study of silicone-modified epoxy resin containing humic acid and other additives. *ACS Appl. Polym. Mater.* **2021**, *3*, 5969–5981. [[CrossRef](#)]
23. Mishra, V.R. Utilization of waste saw dust in development of epoxy resin hybrid green composite. *Mater. Today Proc.* **2020**, *25*, 799–803. [[CrossRef](#)]
24. Beghetto, V.; Sole, R.; Buranello, C.; Al-Abkal, M.; Facchin, M. Recent Advancements in Plastic Packaging Recycling: A Mini-Review. *Materials* **2021**, *14*, 4782. [[CrossRef](#)]
25. He, J.Y.; Xu, P.L.; Zhou, R.; Li, H.; Zu, H.; Zhang, J.; Qin, Y.; Liu, X.; Wang, F. Combustion Synthesized Electrospun InZnO Nanowires for Ultraviolet Photodetectors. *Adv. Electron. Mater.* **2022**, *8*, 2100997. [[CrossRef](#)]

Disclaimer/Publisher's Note: The statements, opinions and data contained in all publications are solely those of the individual author(s) and contributor(s) and not of MDPI and/or the editor(s). MDPI and/or the editor(s) disclaim responsibility for any injury to people or property resulting from any ideas, methods, instructions or products referred to in the content.